Seismic Fragility Analysis of the Smithsonian Institute Museum Support Center

Xin Chu,[a] **S.M.EERI, James M. Ricles,**[a] **M.EERI, and Shamim N. Pakzad**[a]

This paper presents the seismic fragility assessment of the Smithsonian Institute Museum Support Center (MSC), which sustained appreciable damage during the 2011 Virginia earthquake. A three-dimensional (3-D) finite element model (FEM) for the building was created and validated using measured dynamic characteristics determined from field vibration test data. Two suites of bidirectional ground motions at different hazard levels were applied to the FEM to generate fragility curves for structural as well as nonstructural (storage cabinets) damage. The effect of brace yielding strength on structural and nonstructural damage is also investigated to provide recommendations for future retrofit. The fragility curves show that the spectral acceleration to cause structural damage to the building is not high. Due to low seismicity, however, the probability for the structure to be damaged at the design basis earthquake is small. Nevertheless, the probability for nonstructural damage is considerable, which is an important issue related to the seismic performance of the building. [DOI: 10.1193/123115EQS193M]

INTRODUCTION

The magnitude 5.8 (USGS 2011) Mineral, Virginia, earthquake serves as a wake-up call for the engineering community to reflect on the seismic risk for the central and eastern United States (CEUS) region. Earthquakes, despite a low occurrence rate, may still make a broad and pronounced impact to the CEUS communities due to the slow attenuation of earthquake wave in the stable intra-plate environment (Atkinson and Boore 2006, Campbell 2003) and unique geological features that enable a large soil amplification effect (Chapman et al. 2006). In addition, there is a lack of understanding of the seismic resistance of structures in the CEUS which are not designed using stringent seismic design codes such as in California.

The Smithsonian Institute Museum Support Center (MSC), which suffered extensive damage during the Virginia earthquake, exemplifies these concerns. Studies show that the directional attenuation (Chapman 2013) and soil amplification effect (Shahidi et al. 2015) played an important role in the structural damage during the earthquake. In addition, the floor eccentricity that resulted from the distribution of storage content weight is suspected to have contributed to the unique damage pattern in this structure (Chu et al. 2014). However, it remains unclear how vulnerable the structure is and how the structure will perform during a future seismic event. In addition, the MSC is a warehouse facility that is home to numerous

[a] Department of Civil and Environmental Engineering, Lehigh University, 117 ATLSS Drive, Bethlehem, Pa 18015, USA

Earthquake Spectra, Volume 33, No. 1, pages 85–108, February 2017; © 2017, Earthquake Engineering Research Institute

invaluable collections. Hence, the need to preserve the stored artifacts is directly related to the normal functioning of this building. A fragility study for the onset of structural damage as well as the initiation of cabinet motion was therefore conducted so as to explore the seismic risk posed to the structure and its storage contents to enable the Smithsonian Institute to make risk-informed decisions on retrofitting the structure.

The objective of this paper is to develop fragility curves for the building and quantify the risk to the structure in the context of the east coast seismic hazard environment. The paper is organized as follows: It begins with a brief introduction of the building. Then the observations made during the post-Virginia earthquake reconnaissance is presented. Next, 3-D nonlinear finite element modeling of the building is introduced, followed by the validation process. The paper then focuses on the fragility assessment of the structure. Two suites of ground motions each representing a different hazard level were created and applied to the FEM for the purpose of performing nonlinear response time history analysis. Both ground motion suites account for the soil amplification effect. The structural responses are analyzed to generate fragility curves for limit states for structural damage as well as various motions for the different types of storage cabinets. The paper also investigates the effect of retrofitting using stronger steel braces on the fragility of structural and nonstructural damage. In the end, the probability of exceeding these limits at different seismic hazard levels is calculated based on the fragility curves and several conclusions are drawn.

BUILDING DESCRIPTION

The MSC (Figure 1a) is a museum warehouse complex for the conservation, study and storage of the off-display artifacts, which is located in Suitland, MD, approximately 6 miles southeast of Washington, D.C. The 700,000 square feet zigzag-shaped complex is divided into three parts: the five "Pods"; five Offices; and an interconnecting corridor called the "Street" (Figure 1b). The Pods are one-story high bay concrete frames with infilled masonry walls while the Offices are two-story in filled masonry precast concrete frames designed

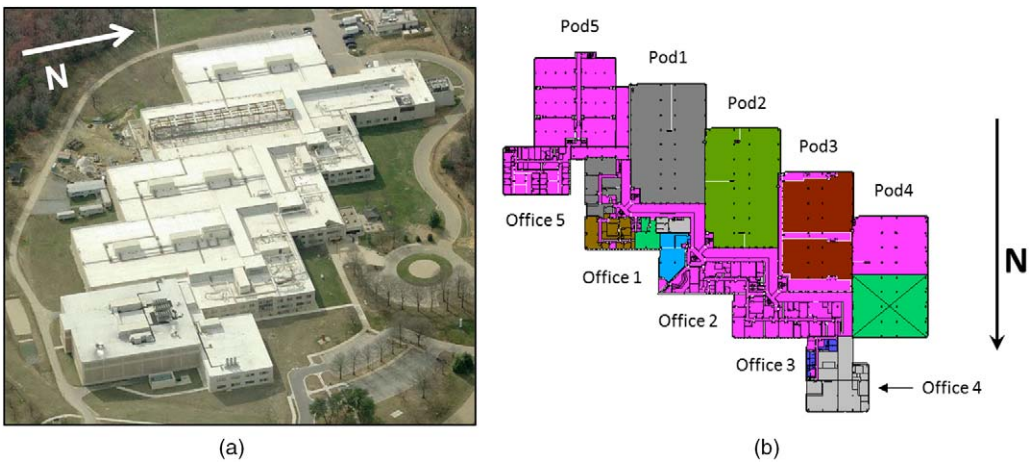

Figure 1. (a) Aerial view of MSC (http://www.bing.com/map); (b) floor plan of MSC.

between 1979 and 1980. More information about the concrete structure can be found in Chu et al. (2014).

Inside each of Pods 1 and 2 is a two-story steel mezzanine that was designed in 1988 and later added to the existing concrete structure. The mezzanine is anchored to the ground floor of the existing concrete structure by expansion bolts. With a two inch gap between the perimeter edge of the floor slabs and the outer masonry walls of the Pod (Figure 2a), the mezzanines are designed and constructed to be structurally independent from the existing concrete frame, except for sharing the same foundation with the concrete structure. The mezzanines are steel concentrically braced frames with diagonal cross bracing in two orthogonal directions of the structure (Figure 2b). As each of the mezzanines has a longer dimension in the N-S direction than the E-W direction (Figure 2b), the N-S direction is referred to as long direction of the building while the E-W direction is defined as short direction. A typical configuration of the braced bays is shown in Figure 2c. The diagonal bracing comprises of A36 steel rectangular bars of $2'' \times 0.25''$ size. The columns are A500

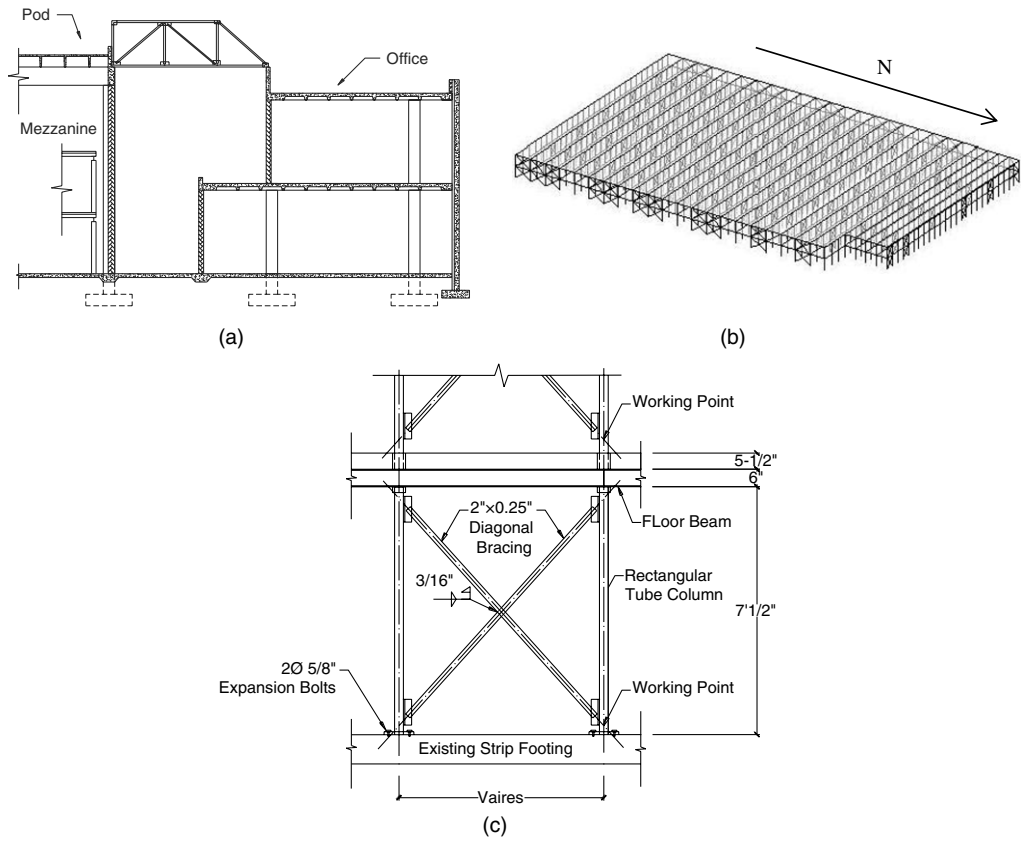

Figure 2. (a) Typical elevation of Pod, Office and mezzanine; (b) steel mezzanine inside Pod; (c) typical braced bay.

(Grade B) steel HSS sections including HSS3 × 3 × 5/16, HSS3 × 3 × 1/4, HSS4 × 2 × 1/4 and HSS6 × 2 × 1/4, while the beams are A36 W shapes including W6 × 9, W6 × 12, W6 × 15, W6 × 20 and W8 × 31. The floor system employs a composite slab with 6″ thick concrete cast on top of metal decking supported by steel beams. The UBC 1985 was employed in the seismic design of the mezzanines.

DAMAGE RECONNAISSANCE

Following the earthquake, damage reconnaissance of the structure was conducted by some of the authors who were the members of an EERI reconnaissance team (Beavers et al. 2012, EERI 2011) as well as subsequent reconnaissance. This section reviews the damage sustained by the structure during the 2011 Virginia earthquake.

The 2011 Virginia earthquake resulted in wide-ranging damage to both the concrete and steel structures of the MSC. Typical damage observed in the concrete frames includes concrete spalling, T-beam sliding at the roof and cracking in the in filled wall (see Figure 3). Failure of a RC beam-column joint was found (Figure 3a) near the roof level at a corner of Office 1. This specific failure consists of concrete spalling at the ends of the beam and columns adjacent to the joint, buckling of the rebar and falling of the tile façade at the upper half of the corner. Figure 3b shows a crack of about ½″ width in a masonry wall of Office 2 which extended throughout the entire height of the second floor. Other observed damage included at least five T beams in different locations having slid from their bearing. For example, Figure 3c shows sliding of a precast roof T-beam in Pod 2 that had slid from its support bearing for about 2 in. Cracks in the masonry wall were also observed in a number of places.

Damage was also observed in both steel mezzanines in Pods 1 and 2. However, the mezzanine in Pod 1 suffered more extensive damage than that in Pod 2. The type of damage included brace buckling and yielding at both stories, in addition to brace facture and anchor bolt failure at the ground level. The second story sustained less damage than the first story,

Figure 3. (a) RC beam-column joint failure; (b) crack in masonry wall; (c) sliding of T beams.

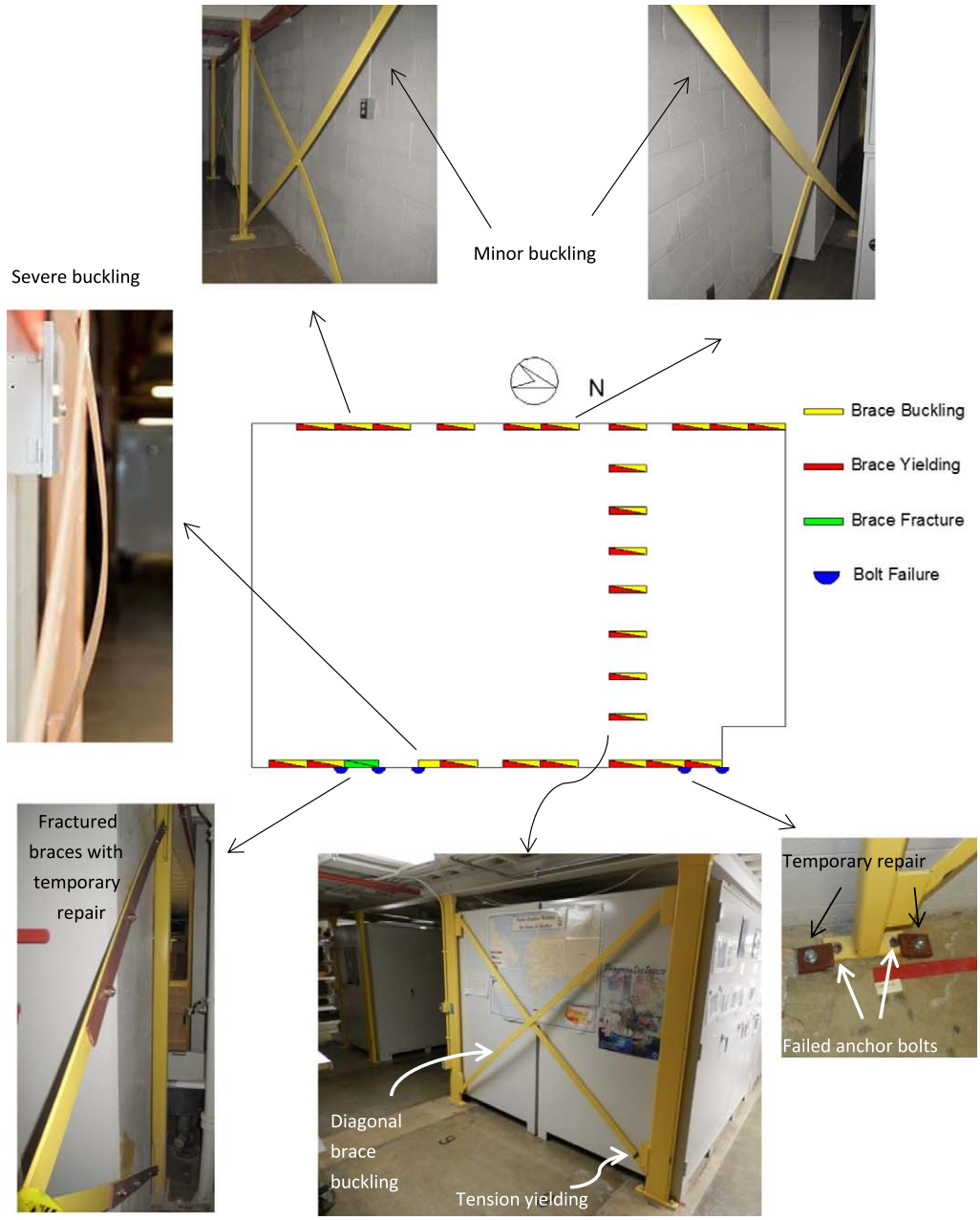

Figure 4. Type and distribution of damage in the first story of the steel mezzanine in Pod 1.

with only some minor yielding and buckling. Figure 4 shows the location and condition of damage of the steel mezzanine in the first story of Pod 1. The braces in the N-S direction of the structure and anchor bolts in some of the braced bays suffered significant damage.

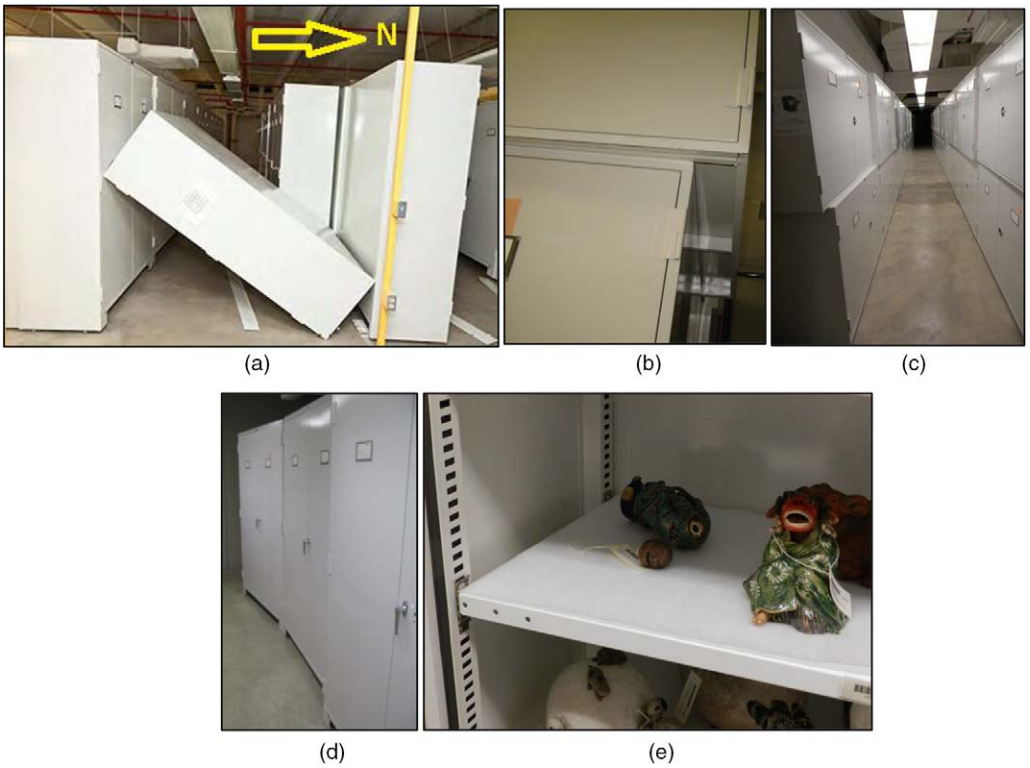

Figure 5. Nonstructural damage: (a) toppling of a storage cabinet; (b) and (c) sliding of cabinet; (d) cabinet dislodged; (e) storage content damage.

In contrast, there were no signs of structural damage in any of the beams or columns and the diagonal braces in the E-W direction of the structure. Among the damaged braces in the N-S direction, those in the east perimeter suffered more significant damage in the form of yielding and buckling than their counterparts along the west perimeter of the structure. In addition, in a braced bay near the southeast corner of the floor plan both diagonal braces had fractured.

The nonstructural (storage content) damage is observed to be mainly associated with the motion of cabinets induced by floor accelerations. The damage can be categorized into rocking (toppling) and sliding. Figure 5a shows the toppling of a cabinet as a consequence of excessive rocking. Figures 5b and 5c show that numerous cabinets stacked on top of other cabinets have slid. Figure 5d shows the dislodging of some cabinets which may be caused by either rocking or sliding. Figure 5e shows a damaged artifact stored in a cabinet as a result of cabinet motion.

FINITE ELEMENT MODELING

The focus of this paper is on the steel mezzanine in Pod 1 which suffered the most severe damage among all parts of the structure. In order to perform the fragility analysis, it is important to model the nonlinear behavior of the structure, which is bound to occur as

structural damage limit states are reached. Thus, a nonlinear model is created in OpenSees (McKenna et al. 2000).

The information obtained from structural drawings was utilized to construct the model. The columns are modeled according to the structural drawings using nonlinear force-based beam-column elements with fiber sections. Due to the composite action of the floor slab and the relatively small stiffness of the columns compared to the beams, the beams are considered axially and flexurally rigid. Therefore, the structure is modeled as a shear building with each floor modeled using a rigid diaphragm constraint. The methodology of Metelli (2013) is used to evaluate the effective slenderness ratio of the diagonal braces which are welded together at the midpoint. The lower limit for the effective slenderness ratio of braces with out-of-plane buckling is calculated assuming a brace buckled in the second mode and the out-of-plane motion at midpoint is zero. Due to the variation of the geometry of each bay, the effective slenderness ratio of the diagonal braces is between 385 and 530, corresponding to a compressive buckling stress of 1.02 to 1.94 ksi (i.e., a buckling load of 0.51 to 0.97 kips). As a result, the straps provide negligible compressive resistance during the earthquake and can be considered to be tension-only members. A combination of a gap element, elastic-no-compression element and nonlinear force-based beam-column element is used in series to model the tension-only behavior of the strap braces (Figure 6). The mass of the structure is considered lumped at the center of mass (CM) at each floor level. Each floor mass weights 2,886.7 kips and is located 122.9 ft. from the south edge and 80.0 ft. from the east edge of the building. More details about the floor mass has been presented in Chu et al. (2014).

MODEL VALIDATION

The model is validated using results from vibration tests and the observed damage pattern (Chu et al. 2014). The modal periods of the OpenSees model is compared with the results from the vibration tests in Table 1 which shows the periods of three identified modes (modes 1, 3, and 5) from these tests.

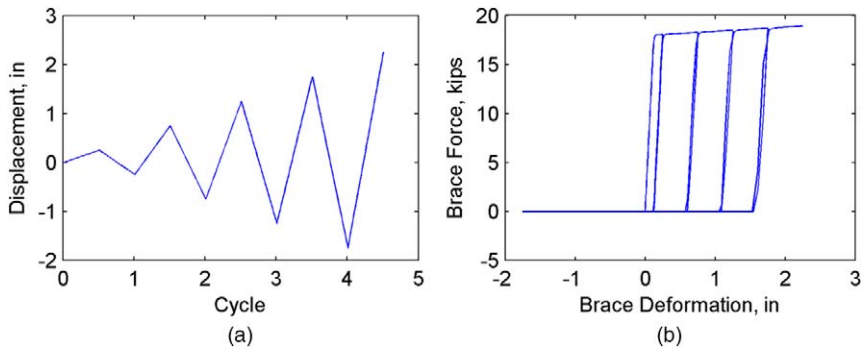

Figure 6. (a) Imposed brace displacement history of displacement-control cyclic load; (b) hysteretic force-displacement response of one diagonal brace (tension force is positive).

Table 1. Comparison of measured and FEM analytical modal periods (unit: s)

		Mode					
	Brace condition	1	2	3	4	5	6
Vibration test data	–	0.30	–	0.21	–	0.11	–
OpenSees model	Post-buckling	0.43	0.33	0.28	0.17	0.13	0.11
	Pre-buckling	0.32	0.25	0.21	0.13	0.10	0.08

OpenSees is able to calculate the modal periods based on the structural stiffness before and after brace buckling by performing an eigen value analysis before and after lateral load is applied to the model. The modal periods of the model with no brace buckling (i.e., pre-buckling) shows better agreement with the test result because the behavior of the braces is amplitude dependent. For the vibration test, the amplitude of the vibration is low and the braces do not buckle and can provide compressive stiffness. However, during seismic excitation the amplitude of vibration is large and the braces buckle (post buckling), and therefore are not able to provide stiffness.

The model is also subjected to ground motions from the 2011 Virginia earthquake. Figure 7 shows the peak axial stress response in the braces in the first story. It presents a pattern consistent with the observation (Figure 4) in which the axial stress in the braces along the east perimeter is larger than that along the west perimeter. The braces in the east perimeter have yielded (exceeding the nominal yield strength 36 ksi).

The model appears to match well with the dynamic properties under low level of vibrations and the observed damage under higher levels of vibration, and therefore deemed suitable for use in the fragility analysis.

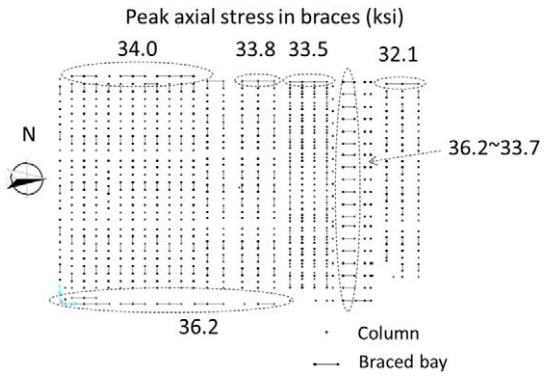

Figure 7. Peak axial stress in braces of first story in response to Virginia earthquake.

FRAGILITY ANALYSIS

One of the key ingredients to systematically evaluate the seismic vulnerability of a structure is to obtain its fragility curve for various limit states. The fragility curves for this study are analytically generated by performing nonlinear response time history analysis using the OpenSees model described in the previous sections and a procedure that is commonly used (Choi et al. 2004, Ellingwood et al. 2007, Pan et al. 2010).

A fragility curve presents the probability that a structure exceeds a certain limit state at a given ground shaking intensity. A fragility function (Equation 1) typically takes the form of a lognormal cumulative distribution function (CDF) and is characterized by two parameters IM_C and β_C, which represent the median structural capacity and lognormal standard deviation that accounts for the uncertainty, respectively:

$$P_f = \Phi\left(\frac{ln(IM/IM_C)}{\beta_C}\right) \tag{1}$$

In Equation 1, IM is the ground shaking Intensity Measure (e.g., spectral acceleration S_a) and Φ is the standard normal CDF.

To obtain the value of IM_C and β_C, the probabilistic seismic demand model (PSDM) which describes the relationship between the ground shaking intensity and the engineering demand parameter (EDP) should be established. The PSDM is generated by performing a regression analysis on the structural responses from nonlinear response time history analyses involving a suite of ground motions. The PSDM in this study follows the form of a power relationship, which is shown to be valid for steel frame structures (Kinali and Ellingwood 2007):

$$\theta_d = aS_a{}^b \tag{2}$$

in which θ_d is seismic demand expressed in terms of EDP; S_a is the spectral acceleration; a and b are coefficients found from a regression analysis.

IM_C is then obtained by back calculating the IM corresponding to the EDP threshold of a limit state using the PSDM. β_C, which describes the uncertainty, should include both aleatoric and epistemic uncertainty, that is, uncertainty in seismic demand σ_d, structural capacity σ_c, and structural modeling σ_m, where:

$$\beta_C = \sqrt{\sigma_d{}^2 + \sigma_c{}^2 + \sigma_m{}^2} \tag{3}$$

GENERATION OF HAZARD COMPATIBLE GROUND MOTION

A major contributor to the uncertainty in the structural response is uncertainty in seismic demand caused by the inherent randomness of the ground motion characteristics. To characterize the uncertainty in seismic demand a suite of ground motions are generated that represent the hazard level, the tectonic environment, and geological features at the site of the structure.

To account for the unique tectonic condition in the East Coast of the United States, the ground motion database developed by McGuire et al. (2001) is utilized. While most of the records in this database come from the West Coast of the United States or a similar tectonically active region, the ground motions have been scaled by applying a transfer function to make them suitable for use in a tectonically inactive environment.

The database contains 151 sets of tri-directional ground motions at the bedrock level. To make those ground motions compatible with the hazard level at the site of the MSC, a scale factor f is found which minimizes the sum of square of the error (SSE) between the target spectrum ${S_a}^{target}$ and the geometric mean spectrum for the two horizontal components of each ground motion set ${S_a}^{record}$ over the period range between 0.0 s to 2.0 s:

$$SSE = \sum_{i=1}^{n} [\ln({S_a}^{target}(T_i)) - \ln(f * {S_a}^{record}(T_i))]^2 \tag{4}$$

in which

$${S_a}^{record}(T_i) = \sqrt{S_{ax}(T_i) \cdot S_{ay}(T_i)} \tag{5}$$

In Equation 4, T_i is the period value between 0.0 to 2.0 s at an interval of 0.01 s, S_{ax} and S_{ay} are the spectral acceleration for the two horizontal components of a record set, f is the scale factor, and n is the total number of discretized periods.

The scale factor is applied to both horizontal components for each ground motion set. In the end, a suite of 22 bidirectional ground motions with the smallest SSE among all the 151 sets are selected as the spectrum compatible bedrock motion for each hazard level. As a result, there is one suite of ground motions for the design basis earthquake (DBE) hazard level and another for the maximum considered earthquake (MCE) hazard level. 22 sets of ground motions are selected in order to be consistent with the methodology in FEMA P-695 (FEMA 2009).

The USGS uniform hazard response spectra (UHRS; Petersen et al. 2008) for the DBE and MCE hazard levels, which correspond to a return period of 475 years and 2,475 years, respectively, at the site of the MSC are employed as the target spectra in selecting the bedrock motions. The site condition for the target spectrum is NEHRP Site Class A (BSSC 2009). As the USGS UHRS provides spectral acceleration values at several discrete points between 0.0 and 2.0 s, this period range is selected for spectrum matching.

Since it has been determined that soil amplification effect played an important role in causing damage to the MSC during the Virginia earthquake (Tilashalski et al. 2015), it is essential to incorporate the effect of the underlying soil in developing the ground motions. To obtain the ground surface motions, a site response analysis is performed on each suite of the selected bedrock ground motions using the open source software DEEPSOIL (Hashash et al. 2014). The soil profile (see Figure 8) is the same as the one used in Chu et al. (2014) that results in a calculated response consistent with the observed damage. The measured shear wave velocity is limited to a soil depth of 82 m, beyond which it is assumed that the shear wave velocity transitions to the bed rock velocity over a soil depth of 165 m. The result of the

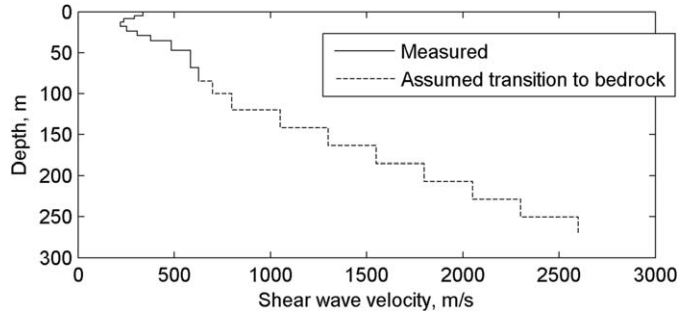

Figure 8. Shear wave velocity profile of soil strata used in site response analysis for records used in fragility analysis.

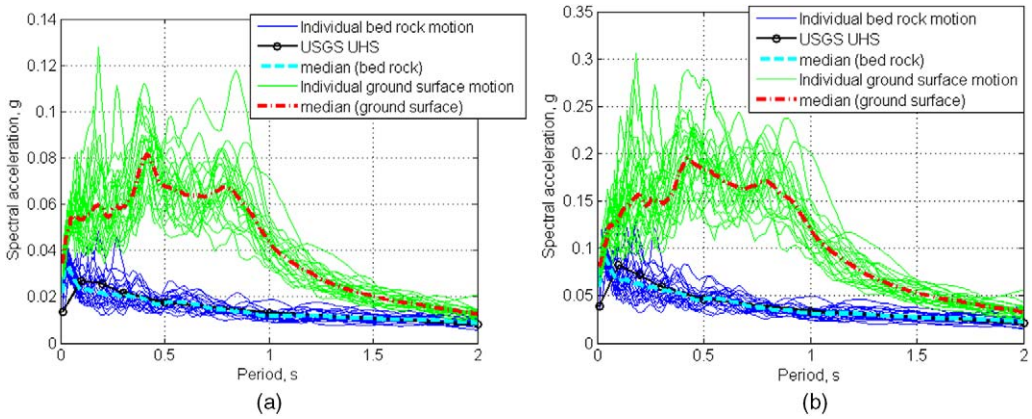

Figure 9. Individual and median value of ensemble of bedrock motion, ground surface motion and target spectrum for (a) DBE hazard level and (b) MCE hazard level.

selected bedrock motion suites and the developed ground surface motion suites for DBE and MCE hazard levels is shown in Figure 9.

The suite of ground surface motions for DBE and MCE hazard levels are used in the nonlinear response time history analyses to generate the fragility curves. To account for the uncertainty in the direction of the earthquake, the two orthogonal components of the ground motion are interchanged with respect to the long and short direction of the building (Peruš and Fajfar 2005). As a result, there are 44 nonlinear response time history analysis for each hazard level.

LIMIT STATE OF STRUCTURAL DAMAGE, EDP AND INTENSITY MEASURE

This study is mainly concerned with the limit state "onset of damage" for the following reasons: (1) damage to the building is of major concern to the stakeholders; (2) the probability

of reaching major damage limit states is low considering the seismicity of East Coast United States.

According to the assessment of the finite element analysis results and observations from the damage reconnaissance, the initial damage in the steel mezzanine is most likely to take place in the diagonal braces. Therefore, the ductility demand on the diagonal braces (Equation 6) is chosen to be the engineering demand parameter (EDP) to characterize the seismic demand on the structure, where the brace ductility demand is defined as:

$$\mu = \frac{\Delta_{max}}{\Delta_{yield}} \tag{6}$$

in which Δ_{max} is the maximum lateral displacement of the bay with diagonal bracing; Δ_{yield} is the lateral displacement of the bay to cause yielding of the brace.

It should be noted that not all of the bays share the same ductility demand because of the torsional response of the building and different configuration of each individual bay. Hence, to account for the performance of the entire structure, the limit state of initiation of damage is considered to be achieved when the maximum ductility demand among all braced bays in the structure reaches the value of 1, that is,

$$max(\mu_i) = 1 \tag{7}$$

in which μ_i is the ductility demand of each individual bay.

Alternatively, the fragility of a selected part of the structure can also be investigated by tracking the maximum ductility demand only in that specific region. In the absence of the material property testing, the yield displacement of each bay is calculated from kinematic relationship using the nominal yield strength of 36 ksi for A36 steel. To account for ground shaking intensity of bidirectional ground motions, a nominal spectral acceleration $S_{a,nom}$ is proposed as follows:

$$S_{a,nom} = \sqrt{S_{a1}(T_1) * S_{a2}(T_2)} \tag{8}$$

in which $S_{a1}(T_1)$ is the spectral acceleration of the ground motion in the long direction of the building at the first mode; $S_{a2}(T_2)$ is the spectral acceleration of the ground motion in the short direction of the building at the second mode.

The basis for Equation 8 is that the first mode of the structure is almost purely translational in the long direction while the second mode is torsional coupled with translation in the short direction (Chu et al. 2014).

DEVELOPMENT OF FRAGILITY CURVE FOR STRUCTURAL DAMAGE

The PSDM is generated by performing a linear regression analysis on the natural log of the bracing maximum ductility demand from the nonlinear response time history analysis and the corresponding nominal spectral acceleration (from Equation 8) to obtain the coefficients a and b appearing in Equation 2. In order to examine the relative vulnerability for different parts of the structure, PSDMs are developed for braces in the long direction of the building,

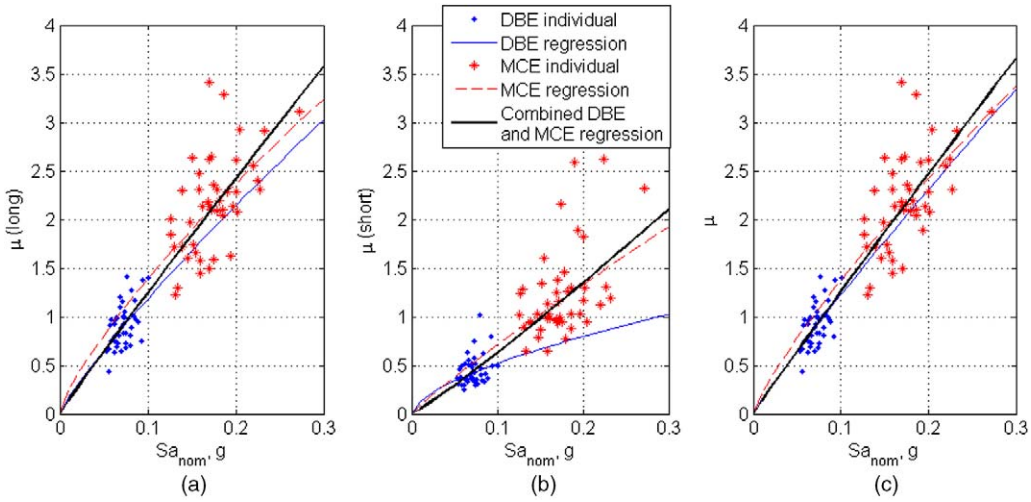

Figure 10. PSDM generated using different ground motions suites for braces in (a) long direction; (b) short direction and (c) combined directions of structure.

short direction of the building, and the entire building (combined directions) by using the structural responses in the corresponding directions. To investigate the effect of the ground motion suite on PSDM, for each part of the structure three PSDMs are determined by using structural response to DBE suite only, MCE suite only and a combination of these two suites, respectively, resulting in the generation of nine PSDMs as presented in Figure 10 and Table 2.

The maximum ductility demand for braces in the short direction is smaller than those in the long direction. As a result, the PSDM for the combined directions is almost the same with that for the long direction. The minor difference is caused by a few cases in which the maximum ductility demand occurs in the short direction of the building as opposed to the long direction.

Another observation from Figure 10 is that the PSDM generated using response from different suites of ground motions is noticeably different. The PSDM generated using the combined suite of DBE and MCE is more similar to those generated using only the

Table 2. Coefficient for PSDM (in the form of Equation 2) for different cases

Coefficient	Direction	DBE suite	MCE suite	Combined suites
a	Long	8.469	8.221	11.358
	Short	2.144	5.73	7.903
	Combined	10.08	9.039	11.796
b	Long	0.854	0.772	0.961
	Short	0.616	0.907	1.100
	Combined	0.916	0.818	0.973

DBE suite when the ground shaking intensity is low, while they are more similar to those generated from MCE suite when the ground shaking intensity is high.

Fragility curves are generated based on the PSDM obtained above using the combined suites for the DBE and MCE ground motions. Due to lack of material testing, the variability for material strength cannot be established. In addition, Celik and Ellingwood (2010) suggested the uncertainty in material strength makes limited difference in fragility analysis in CEUS structures. Therefore, the material strength in this study is treated as deterministic and the term to describe the uncertainty of structural capacity σ_c in Equation 3 is set equal to zero. The uncertainty in finite element modeling σ_m in this same equation is set equal to 0.2, as suggested by Kinali and Ellingwood (2007).

Figure 11 shows the fragility curves for the onset of damage for the long direction, short direction and combined directions of the structure. Table 3 shows the coefficients for the fragility function in Equation 1. The long direction of the structure is more fragile than the short direction. At the ground shaking intensity of the Virginia earthquake whose nominal spectral acceleration Sa_{nom} based on Equation 8 is 0.09 g, the long direction of the structure has a probability of 0.660 of sustaining damage while the short direction has a probability of only 0.054 of being damaged. The ground shaking level corresponding to a 50% probability of damage in the combined directions of the structure is small (0.079 g). The probability of damage occurring in the combined directions of the structure is close to that for the long direction, corroborating with the previous conclusion that damage is much more likely to take place in the long direction of the structure.

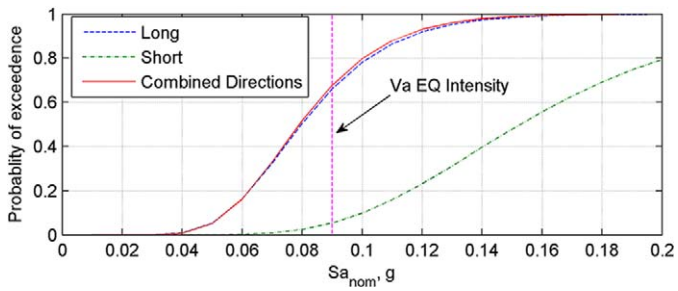

Figure 11. Fragility curve for different parts of the structure for onset of damage.

Table 3. Coefficients for fragility function shown in Figure 11

	IM_c	β_c
Long	0.0798	0.2907
Short	0.1527	0.329
Combined directions	0.0791	0.281

FRAGILITY CURVE FOR NONSTRUCTURAL DAMAGE

Since the purpose of the MSC is to provide storage to preserve artifacts, it is therefore important to investigate how safe the artifacts are during a future earthquake. The methodology to assess the safety of the artifacts during an earthquake is to develop fragility curves associated with the initiation of cabinet motion. Motion of the cabinet can lead to its contents being damaged from impact with other artifacts within the cabinet, or impact with the cabinet.

Cabinet motions are induced by floor acceleration. Based on physical principles, Shenton III (1996) developed criteria to initiate different kinds of motion for a rigid body resting on the ground subjected to ground acceleration. Depending on the floor acceleration intensity (a_{max}), coefficient of friction (μ_s) between the cabinet and the surface it rests on, the location of center of gravity (β) and the aspect ratio (width-to-height, B/H), the cabinet may remain at rest, rock, or slide. Figure 12a shows the criteria in parameter space for a cabinet with its center of gravity located at βH from its bottom and an aspect ratio of 3. The definition of various parameters is illustrated in Figure 12b. The Slide & Rock region identified in Figure 12a is a motion in which rocking occurs initially, but is proceeded by sliding as the friction force diminishes. The other regions in Figure 12a indicate the respective condition of the cabinet for a given set of parameters.

According to these criteria, the fragility function for the rocking and sliding of a cabinet can be defined as follows:

$$F_{rocking}(S_a) = P\left[\left(a_{max} > \frac{B}{2\beta H}g\right) \cap \left(\mu_s > \frac{B}{2\beta H}\right) \mid S_a\right] \tag{9}$$

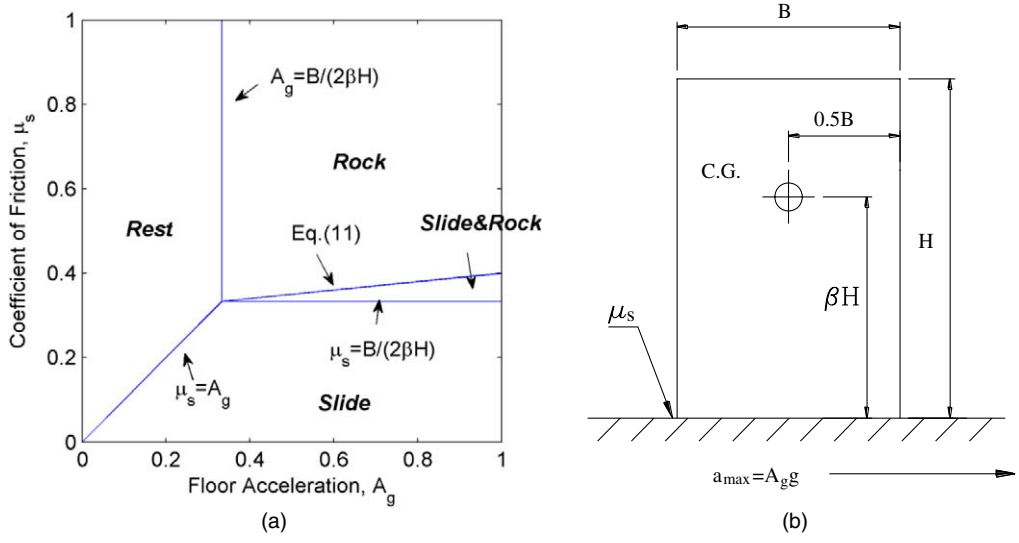

Figure 12. (a) Criteria for different types of motion in parameter space; (b) definition of various parameters.

$$F_{sliding}(S_a) = P\left\{\left[(a_{max} > \mu_s g) \cap \left(\mu_s < \frac{B}{2\beta H}\right)\right] \cup \left[(a_{max} > A_g{}^*) \cap \left(\mu_s > \frac{B}{2\beta H}\right)\right] \,\middle|\, S_a\right\} \tag{10}$$

in which S_a is the spectral acceleration associated with the ground shaking intensity; a_{max} is the maximum floor acceleration; g is the gravity acceleration, and $A_g{}^*$ is defined as:

$$A_g{}^* = \frac{(1+4\gamma^2)\mu_s - 3\gamma}{4+\gamma^2-3\gamma\mu_s} \tag{11}$$

$$\gamma = \frac{B}{2\beta H} \tag{12}$$

It should be noted that a_{max} is chosen to be the maximum floor acceleration in the N-S direction of the building in order to be compatible with the 1-D nature of the criteria developed in Shenton III (1996). The reason to choose the N-S direction as opposed to the E-W direction is because a cabinet is more likely to rock in the N-S direction due to the short direction of the cabinets being orientation in that direction (Figure 5a).

Similar to the approach to establish the PSDM for structural damage, a regression analysis is performed to develop the PSDM for maximum floor acceleration. The regressed relation for the second floor absolute acceleration in the long direction is shown in Figure 13 and expressed by Equation 13 which gives the median value of maximum floor acceleration conditioned on the spectral acceleration. The second floor absolute accelerations were obtained from the nonlinear response time history analysis. The dispersion from the regression analysis is found to be 0.192 which is the lognormal standard deviation of the floor acceleration demand.

$$a_{max} = 0.95 Sa_{nom}{}^{0.65} \tag{13}$$

One of the important aspects in studying the fragility of these cabinets is the uncertainty on the capacity of the cabinets against motion, which is a result of the uncertainty in the coefficient of friction and the location of center of gravity. It is assumed that the coefficient of friction μ_s and the normalized height of the center of gravity β follow a normal distribution.

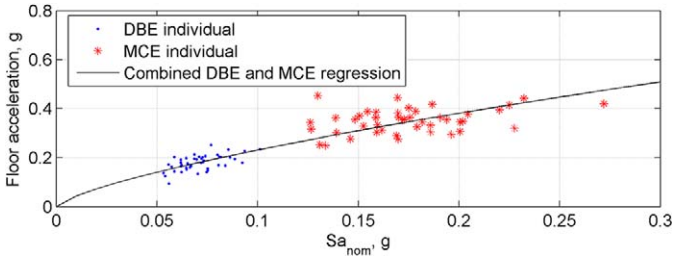

Figure 13. PSDM for maximum floor acceleration in the NS direction of the second floor.

Table 4. Dimension and friction property of the different types of cabinets

				Friction			Height of center of gravity	
					μ_s		β	
Type	B (in.)	H (in.)	B/H	Contact surface material	Mean	Standard deviation	Mean	Standard deviation
348	22.6	81.5	0.277	Steel-concrete	0.6	0.15	0.5	0.1
220	38.6	40.75	0.947	Steel-steel	0.15	0.05	0.5	0.1
395	50	81.5	0.613	Steel-concrete	0.6	0.15	0.5	0.1

There are three types of cabinets in Pod 1: Type 348 (Figure 5a and 5d), Type 220 (Figure 5b and 5c) and Type 395 (bottom middle photograph in Figure 4). Table 4 lists their dimensions and friction properties. Dimensions of the cabinets were provided by MSC staff (Dietrich 2012). The mean value and standard deviation for the coefficient of friction are based on previous studies by Rabbat and Russell (1985) and Dooley (1957). It should be noted that the Type 220 cabinets are stacked on top of each other. The cabinets in the upper stack are selected for the study because the reduced coefficient of friction that exists between the steel-to-steel contact surface renders them more vulnerable to sliding.

Due to complex criteria involved in defining the initiation of cabinet motion, an analytical expression for the fragility function (Equations 9 and 10) is difficult to obtain. As a result, a Monte Carlo simulation approach is employed to calculate the fragility function. For a given ground shaking intensity S_a, one million samples of floor acceleration demand a_{max} are generated using the developed PSDM (Equation 13) along with the coefficient of friction (μ) and normalized height of center of gravity (β) using the normal distribution with the parameters specified in Table 4. The probability that motion is initiated can be calculated by dividing the number of samples that satisfy the corresponding criteria by the total number of samples. By repeating this process for a range of ground shaking intensity, the entire fragility curve can be developed numerically.

Figure 14 shows the probability of initiation of rocking and sliding for the three different types of cabinets that were obtained from the Monte Carlo simulations. It can be seen that Type 348 cabinet (Figure 5a) has the highest probability to rock. This is attributed to the large aspect ratio of this type of cabinet. On the contrary, Type 220 (Figure 5b and 5c) has a low probability to rock due to its small aspect ratio. However, the probability of sliding is the highest among the three types of cabinets. This is due to the smaller coefficient of friction of the painted steel-to-steel contact surface of Type 220 cabinets. Type 395 has a smaller aspect ratio than Type 348 and a contact surface of steel and concrete, making its probability of both sliding and rocking moderate. It should be noted that the fragility curve does not resemble a conventional fragility curve that takes the form of a lognormal CDF. The reason is that, as explained above, the coefficient of friction, cabinet aspect ratio and center of gravity, and level of floor acceleration have an effect on the type of motion that a cabinet develops. For example, if the ground acceleration is large the probability that a Type 348 cabinet will rock

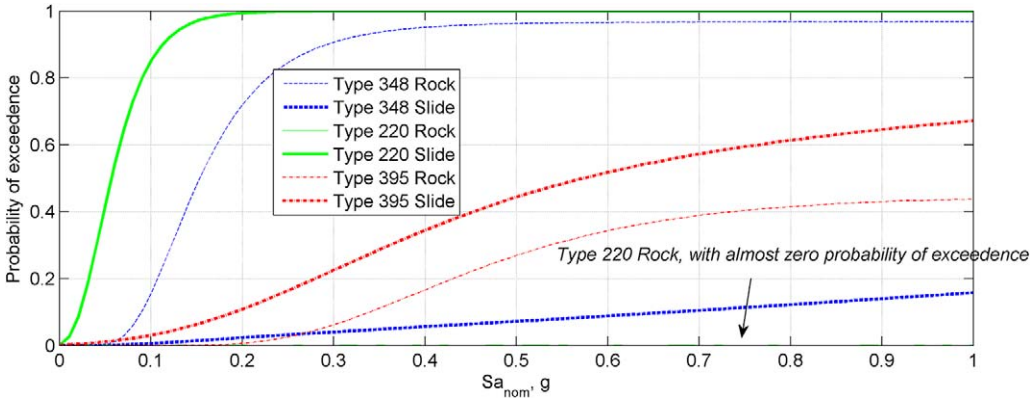

Figure 14. Fragility curves for initiation of motion for different types of cabinets.

cannot be one hundred percent if the coefficient of friction is small, as the cabinet will have the tendency to slide and not rock (Figure 12a). The uncertainty in the coefficient of friction keeps the probability of rocking from reaching one. In addition, the various uncertain parameters that determine the capacity of the cabinets against motion also do not follow a log-normal distribution.

RETROFIT OF STRUCTURE

The Smithsonian Institute is considering to seismically retrofit the mezzanine by replacing the diagonal strap braces with high strength steel cables with sufficient pretension to make them taut. The objective is to make the structure stronger and have less structural damage under a similar future earthquake. Past experience however shows that if a structure remains linear during an earthquake that the floor acceleration demand will increase. For the MSC, this will increase the probability for the storage contents in the cabinets to be damaged. Thus the FEM is modified with increased brace yield strength to investigate its effect on the floor acceleration. Two cases are studied: one with brace yield stress of 72 ksi; the other with 150 ksi.

It was found from the subsequent nonlinear response time history analysis that were performed that for the case of 72 ksi yield strength that there are only a few ground motions that cause the braces to yield. However in the latter case (150 ksi yield strength), no brace yields under all of the considered earthquakes. The results of the floor acceleration PSDM along with the original case ($F_y = 36$ ksi) are shown in Figure 15 and Table 5. Figure 15 shows that by increasing the yield stress of the bracing, the floor acceleration demand has increased significantly, especially at a higher level of ground shaking intensity. Using the results for the PSDM for floor acceleration, the fragility of the cabinets for these different cases can be compared. Figure 16 shows the fragility curve for cabinet sliding and rocking limit states for different types of cabinet.

Increasing the brace yield strength causes the fragility of the cabinet to significantly increase. Considering that the braces are designed to yield and dissipate energy, the damage of bracing is acceptable. The purpose of the MSC is to preserve storage content. Thus it is

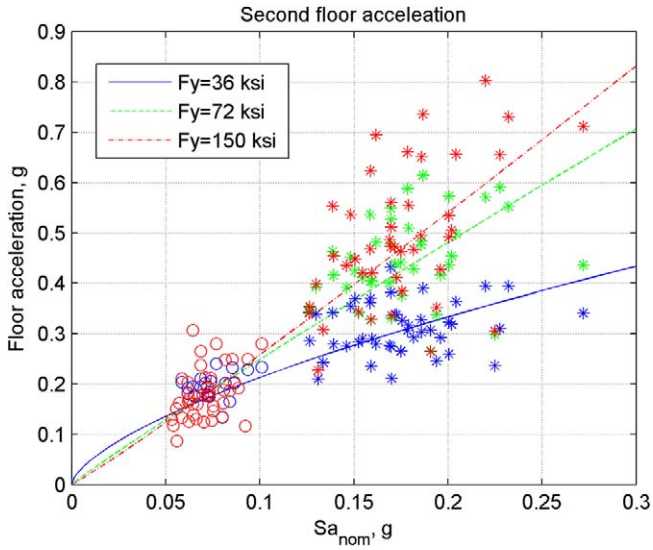

Figure 15. PSDM for floor acceleration for structures using braces of different yield strength.

more important to keep the floor acceleration demand low by using a low yield strength to allow the braces to yield. Therefore, it is not recommended to retrofit the structure with high strength braces. Studies have shown that passive dampers are cost effective in reducing both story drift level and floor acceleration demand (Dong et al. 2016) and could be considered as possible alternative retrofit strategy. It is beyond the scope of this paper however to study this type of retrofit.

PROBABILITY OF EXCEEDING VARIOUS LIMIT STATES

To put the fragility curves in Figure 11 and Figure 14 into perspective, the nominal spectral accelerations are calculated from the USGS UHRS (Petersen et al. 2008) for the DBE and MCE level using Equation 8. Using an actual ground motion, the nominal spectral acceleration of the Virginia earthquake is determined as well. Hence the probability of exceeding various limit states under various hazard levels can be assessed. The USGS spectrum originally provides spectral acceleration for Site Class B. To account for the soil amplification effect, the spectral acceleration is multiplied by the soil amplification factor Fa = 1.6 from the building code (ASCE 2010). The Virginia earthquake is believed to have a

Table 5. Parameters for different PSDM for floor acceleration (in the form of $a_{max} = aS_a{}^b$)

Brace yield stress (ksi)	a	b
36	0.9454	0.6469
72	2.221	0.9503
150	3.001	1.065

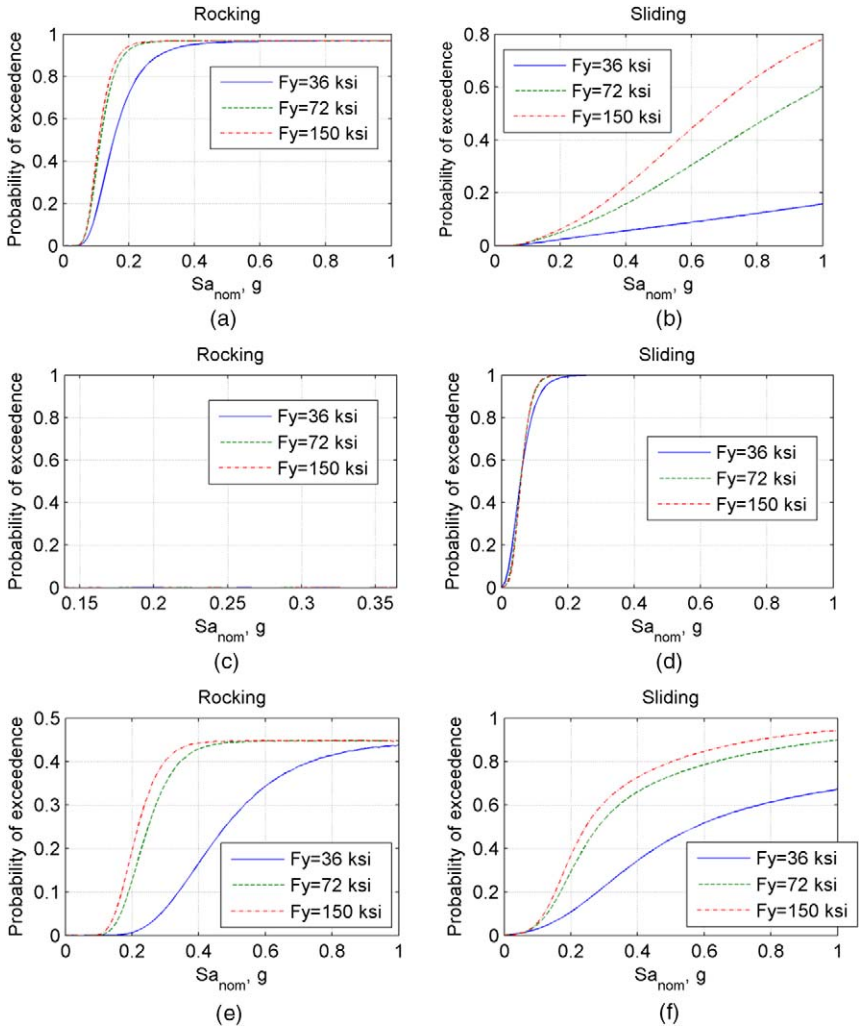

Figure 16. Cabinet fragility curves for structures using braces of different yield strength: (a) Type 348 rocking; (b) Type 348 sliding; (c) Type 220 rocking; (d) Type 220 sliding; (e) Type 395 rocking; (f) Type 395 sliding.

return period of 752 years (Chapman 2015). Plugging in the ground shaking intensity to the fragility curves developed in the previous sections, the probability of exceeding various limit states under different hazard levels are obtained and summarized in Table 6.

At the DBE level, the probability for the building to have structural damage is small (0.068). However, the probability to cause Type 220 cabinets to slide is considerable (0.431). At the MCE level, the structure is almost certain to have structural damage and sliding for Type 220 cabinets to occur. The probability for cabinet 348 to rock is also high under the MCE. At the ground shaking intensity of the Virginia earthquake,

Table 6. Probability of exceeding various limit states at different hazard level

Hazard level (Return period)	Sa_{nom},g	Probability of structural damage	Probability of nonstructural damage					
			Rocking			Sliding		
			Type 220	Type 348	Type 395	Type 220	Type 348	Type 395
DBE (475 years)	0.052	0.068	0	0.004	0	0.431	0.001	0
MCE (2,475 years)	0.139	0.978	0	0.420	0	0.960	0.013	0.019
Virginia 2011 (752 years)	0.09	0.677	0	0.103	0	0.802	0.005	0.005

there is a relatively high probability for structural damage (0.677) and sliding of Type 220 cabinets (0.802) to occur. In addition, there is a considerable probability (0.103) for Type 348 cabinets to undergo rocking. At all hazard levels, the probability for motion to occur in Type 395 cabinets is small.

SUMMARY AND CONCLUSIONS

This paper performs a systematic seismic fragility assessment of the steel mezzanine in Pod 1 of the MSC located in Suitland, Maryland. The structural as well as nonstructural damage reconnaissance following the 2011 Mineral, Virginia, earthquake is reviewed. A nonlinear FEM was developed for the purpose of performing the fragility analysis. The model was validated using the results from a field vibration test as well as the observed damage pattern form the earthquake. To perform the fragility analysis, two suites of hazard compatible ground motions were selected from a CEUS ground motion database. The effect of soil amplification is accounted for by a site response analysis. The suites of ground motion are applied to the FEM for conducting the nonlinear response time history analysis, whose results are used to generate fragility curves. Fragility curves are developed for initiation of structural damage and acceleration-induced motion (rocking and sliding) for different types of storage cabinets in the MSC. The structural damage fragility for different parts of the structure is also studied. The effect of employing braces with different strength in possible seismic retrofit is investigated. The probability of exceeding various limit states at different hazard levels is determined to evaluate seismic risk.

It is found that the structure is more fragile in the N-S direction than the E-W direction. It is also discovered that increasing the yield strength of the braces will significantly increase the floor acceleration demand and thus increase the fragility of the contents in the cabinets.

It is discovered that the ground motion to cause structural damage in the mezzanine is not high. However, due to the low seismic hazard level at the site of MSC, the probability of structural damage to occur during the DBE is small. Considering the fact that both current and traditional seismic design practice in the U.S. employ a reduced seismic design force to exploit the ductility of the structure, damage is expected to occur at the DBE hazard level. The acceptable amount for the probability of structural damage to occur should be determined by the owner of the building, as the repair process following structural damage may affect access to the stored artifacts.

There is a considerable probability that Type 220 cabinet will slide under the DBE earthquake. In addition, at ground shaking intensity of the 2011 Virginia earthquake, Type 348 cabinets also have an appreciable probability of rocking, which is detrimental to the storage contents. Considering that the purpose of the MSC is to preserve the invaluable museum collections, this might pose significant risk in terms of the normal functioning of this storage warehouse. This also reveals the threat faced by a large number of warehouses located in the East Coast U.S. that do not possess measures to secure motions of storage contents, like connecting straps or restraining nets to avoid their motions. As there is no clear specification in building codes on the expected performance of the storage content in museum warehouses, this paper simply provides the probability of possible content damage at different hazard level. It is up to the stakeholder whether such risk is acceptable and if any measures should be taken.

ACKNOWLEDGMENTS

The research reported in this paper is supported by National Science Foundation Award No. CMMI-1219447 and CMMI-1219473. The authors are grateful for the staff at the Smithsonian Institute and the MSC for their help during several field visits. The authors also appreciate the effort from the EERI damage reconnaissance team. The authors also express gratitude to Professor James R. Martin in Clemson University for his help in setting up the field testing and interpreting the results for the site response analysis. The authors want to thank the following students for their help in the field test: Golnaz Shahidi, Hillary Brooker, and Mallory Nigro. Special thanks go to Mr. Robert Kayen from USGS who provided measured soil profile data underneath the MSC. The support of DIGITEXX Data Systems who partially provided the wired instrumentation system is acknowledged.

REFERENCES

American Society of Civil Engineers (ASCE), 2010. *ASCE 7-10: Minimum Design Loads for Buildings and Other*, Reston, VA.

Atkinson, G. M., and Boore, D. M., 2006. Earthquake ground-motion prediction equations for eastern North America, *Bulletin of the Seismological Society of America* **96**, 2181–2205.

Beavers, J. E., Eatherton, M. R., Gilsanz, R. E., Ricles, J. M., and Lin, Y., 2012. The August 23, 2011 magnitude 5.8 Virginia earthquake in the eastern United States: An engineering perspective, *Proceedings of 15th World Conference on Earthquake Engineering*, Lisbon, Portugal.

Building Seismic Safety Council (BSSC), 2009. *NEHRP Recommended Provisions for Seismic Regulations for New Buildings and Other Structures*, Washington, D.C.

Campbell, K. W., 2003. Prediction of strong ground motion using the hybrid empirical method and its use in the development of ground-motion (attenuation) relations in eastern North America, *Bulletin of the Seismological Society of America* **93**, 1012–1033.

Celik, O. C., and Ellingwood, B. R., 2010. Seismic fragilities for non-ductile reinforced concrete frames – Role of aleatoric and epistemic uncertainties, *Structural Safety* **32**, 1–12.

Chapman, M. C., 2013. On the Rupture Process of the 23 August 2011 Virginia earthquake, *Bulletin of the Seismological Society of America* **103**, 613–628.

Chapman, M. C., 2015. Magnitude, recurrence interval, and near-source ground-motion modeling of the Mineral, Virginia, earthquake of 23 August 2011, *Geological Society of America Special Papers*, Geological Society of America, 509, SPE509-02.

Chapman, M. C., Martin, J. R., Olgun, C. G., and Beale, J. N., 2006. Site-response models for Charleston, South Carolina, and vicinity developed from shallow geotechnical investigations, *Bulletin of the Seismological Society of America* **96**, 467–489.

Choi, E., DesRoches, R., and Nielson, B., 2004. Seismic fragility of typical bridges in moderate seismic zones, *Engineering Structures* **26**, 187–199.

Chu, X., Ricles, J. M., Pakzad, S. N., Martin, J. R., and Shahidi, S. G., 2014. Damage reconnaissance and seismic response prediction of an East Coast U.S. building subjected to 2011 Virginia earthquake, *ASCE Structures Congress Proceedings*, Boston, MA, 1324–1335.

Dietrich, E., 2012. Personal communication.

Dong, B., Sause, R., and Ricles, J. M., 2016. Seismic response and performance of a steel MRF Building with nonlinear viscous dampers under DBE and MCE, *Journal of Structural Engineering* **142**, 04016023.

Dooley, R. T., 1957. *Coefficient of Friction of Painted Structural Steel Surfaces*, Georgia Institute of Technology.

Earthquake Engineering Research Institute (EERI), 2011. *Learning from Earthquakes: The Mw 5.8 Virginia Earthquake of August 23, 2011*, EERI Special Earthquake Report, Oakland, CA.

Ellingwood, B. R., Celik, O. C., and Kinali, K., 2007. Fragility assessment of building structural systems in Mid-America, *Earthquake Engineering & Structural Dynamics* **36**, 1935–1952.

Federal Emergency Management Agency (FEMA), 2009. *Quantification of Building Seismic Performance Factors (FEMA P695)*, Washington, D.C.

Hashash, Y. M. A., Groholski, D. R., and Phillips, C., 2014. *DEEPSOIL v5.1 User Manual and Tutorial*, Urbana, IL.

Kinali, K., and Ellingwood, B. R., 2007. Seismic fragility assessment of steel frames for consequence-based engineering: A case study for Memphis, TN, *Engineering Structures* **29**, 1115–1127.

McGuire, R. K., Silva, Walter, J., and Costantino, C. J., 2001. *Technical Basis for Revision of Regulatory Guidance on Design Ground Motions*, Rpt. NUREG/CR-6728, Washington D.C.

McKenna, F., Fenves, G. L., and Scott, M. H., 2000. *Manual of Open System for Earthquake Engineering (Opensees)*, Pacific Earthquake Engineering Research Center, University of California, Berkeley.

Metelli, G., 2013. Theoretical and experimental study on the cyclic behaviour of X braced steel frames, *Engineering Structures* **46**, 763–773.

Pan, Y., Agrawal, A. K., Ghosn, M., and Alampalli, S., 2010. Seismic fragility of multispan simply supported steel highway bridges in New York state. II: Fragility analysis, fragility curves, and fragility surfaces, *Journal of Bridge Engineering*, ASCE, **15**, 462–472.

Peruš, I., and Fajfar, P., 2005. On the inelastic torsional response of single-storey structures under bi-axial excitation, *Earthquake Engineering & Structural Dynamics* **34**, 931–941.

Petersen, M. D., Frankel, A. D., Harmsen, S. C., Mueller, C. S., Haller, K. M., Wheeler, R. L., Wesson, R. L., Zeng, Y., Boyd, O. S., Perkins, D. M., Luco, N., Field, E. H., Wills, C. J., and Rukstales, K. S., 2008. *USGS Open-File Report 2008-1128: Documentation for the 2008 Update of the United States National Seismic Hazard Maps*.

Rabbat, B. G., and Russell, H. G., 1985. Friction coefficient of steel on concrete or grout, *Journal of Structural Engineering*, ASCE, **111**.

Shahidi, S. G., Pakzad, S. N., Ricles, J. M., Martin, J. R., Olgun, C. G., and Godfrey, E. A., 2015. Behavior and damage of the Washington Monument during the 2011 Mineral, Virginia,

earthquake, *Geological Society of America Special Papers*, Geological Society of America, **509**, 235–252.

Shenton, III, H. W., 1996. Criteria for initiation of slide, rock, and slide-rock rigid-body modes, *Journal of Engineering Mechanics*, ASCE, **122**, 690–693.

Tilashalski, M., Guney Olgun, C., Rodriguez-Marek, A., Godfrey, E. A., Chapman, M. C., Shamsalsadati, S., and Eddy, M. A., 2015. Regional geology and seismic site amplification in the Washington, D.C., metropolitan area, *IFCEE 2015*, ASCE, 1278–1287.

U.S. Geological Survey (USGS), 2011. *Magnitude 5.8 - VIRGINIA: Summary*, available at <http://earthquake.usgs.gov/earthquakes/eqinthenews/2011/se082311a/> (last accessed 18 December 2015).

(Received 31 December 2015; accepted 17 August 2016)